DispatchDate: 22.09.2020 · ProofNo: 484, p.1

nature electronics

ARTICLES

https://doi.org/10.1038/s41928-020-00484-7

Check for updates

100 GHz zinc oxide Schottky diodes processed from solution on a wafer scale

Dimitra G. Georgiadou[1,6]✉, James Semple[1], Abhay A. Sagade[2], Henrik Forstén[3], Pekka Rantakari[3], Yen-Hung Lin[1,7], Feras Alkhalil[4], Akmaral Seitkhan[5], Kalaivanan Loganathan[5], Hendrik Faber[5] and Thomas D. Anthopoulos[1,5]✉

Inexpensive radiofrequency devices that can meet the ultrahigh-frequency needs of fifth- and sixth-generation wireless telecommunication networks are required. However, combining high performance with cost-effective scalable manufacturing has proved challenging. Here, we report the fabrication of solution-processed zinc oxide Schottky diodes that can operate in microwave and millimetre-wave frequency bands. The fully coplanar diodes are prepared using wafer-scale adhesion lithography to pattern two asymmetric metal electrodes separated by a gap of around 15 nm, and are completed with the deposition of a zinc oxide or aluminium-doped ZnO layer from solution. The Schottky diodes exhibit a maximum intrinsic cutoff frequency in excess of 100 GHz, and when integrated with other passive components yield radiofrequency energy-harvesting circuits that are capable of delivering output voltages of 600 mV and 260 mV at 2.45 GHz and 10 GHz, respectively.

The fifth generation (5G) of mobile and wireless communications platforms is on the verge of full-scale commercialization. 5G networks mainly operate in three allocated frequency bands: sub-1 GHz (400 and 700–900 MHz), mid-band, 1–6 GHz (specifically around 3.5 GHz), and millimetre waves (mmWave), 20–80 GHz (26–29, 37–40 and 66–71 GHz) (ref. [1]). International standardization of these frequency bands should allow for the prompt development of a holistic 5G era that extends beyond mobile communications towards smart homes, smart factories, virtual reality and vehicle connectivity[2]. Building on the technical breakthroughs that should make such services a reality, preparation for the sixth generation (6G) of wireless communications is now underway[3]. This is expected to enable more sophisticated applications, such as medical imaging and augmented reality, as well as visible light communication and artificial-intelligence-based communication.

6G networks will provide increased speed and capacity, and will probably utilize a multiband higher-frequency spectrum by employing, for instance, combinatorial use of the 1–3-GHz band, mmWave band (30–300 GHz) and terahertz band (0.3–10 THz) (ref. [4]). However, incomplete use of full-band access technology by the existing hardware for high-frequency equipment is currently an issue, as some devices do not support high-frequency bandwidth, and many aspects of the technology are still at the stage of scientific exploration[5]. Some progress has been made with photonic-based approaches[6], but electronics (currently largely based on the III–V semiconductor industry) are still lagging in this frequency range.

As we move to higher carrier frequencies, there are also severe propagation losses, reducing the transmission range and the emitted power, while making device integration significantly more complex and costly. Devices operating at mmWave are mainly targeting networks that are more suitable for indoor applications (below 10 m), and those that are usually applied in chip-to-chip communication and in-body applications or wearable electronics (below 1 m). High-efficiency radiofrequency devices that are lightweight, have a conformal geometry and can be fabricated at low cost are thus currently much sought after.

Schottky diodes are ideal for use in rectifier circuits (such as power detectors, mixers and frequency multipliers) operating at frequencies up to terahertz, which are relevant to wireless communication systems and also energy-harvesting applications. By carefully engineering the Schottky barrier at the metal–semiconductor junction, a low voltage drop can be obtained. Their unipolar operation, involving only majority carriers, means that negligible storage of excess minority carriers occurs, leading to small capacitances that can further boost their operating frequency. Terahertz rectifiers based on a graphene–SiC materials platform were recently reported[7]. However, the high temperatures involved in their fabrication (thermal annealing at 1,700 °C) renders the technology impractical for large-volume, inexpensive applications, and incompatible with flexible commodity substrate materials, such as polymers.

There has been increasing interest in Schottky diodes based on amorphous oxides, such as indium gallium zinc oxide, in the last decade. They have been shown to operate at frequencies reaching 4.2 GHz, mainly due to their high electron mobility, and offer low device-to-device variability, ease of processing, and compatibility with plastic substrates and flexible electronics applications[8]. Zinc oxide is another low-cost abundant compound semiconductor that can be processed from solution on inexpensive temperature-sensitive substrate materials. However, operation of ZnO diodes is so far limited to the commercially relevant high-frequency radiofrequency identification and near-field communications band of 13.56 MHz (refs. [9,10]).

[1]Department of Physics & Centre for Plastic Electronics, Imperial College London, London, UK. [2]Laboratory for Advanced Nanoelectronic Devices, Department of Physics and Nanotechnology, SRM Institute of Science and Technology, Kattankulathur, Tamil Nadu, India. [3]VTT Technical Research Centre of Finland, Espoo, Finland. [4]PragmatIC, Cambridge, UK. [5]Division of Physical Sciences and Engineering, King Abdullah University of Science and Technology (KAUST), Thuwal, Saudi Arabia. [6]Present address: Zepler Institute for Photonics and Nanoelectronics, University of Southampton, Southampton, UK. [7]Present address: Clarendon Laboratory, Department of Physics, University of Oxford, Oxford, UK. ✉e-mail: D.Georgiadou@soton.ac.uk; thomas.anthopoulos@kaust.edu.sa

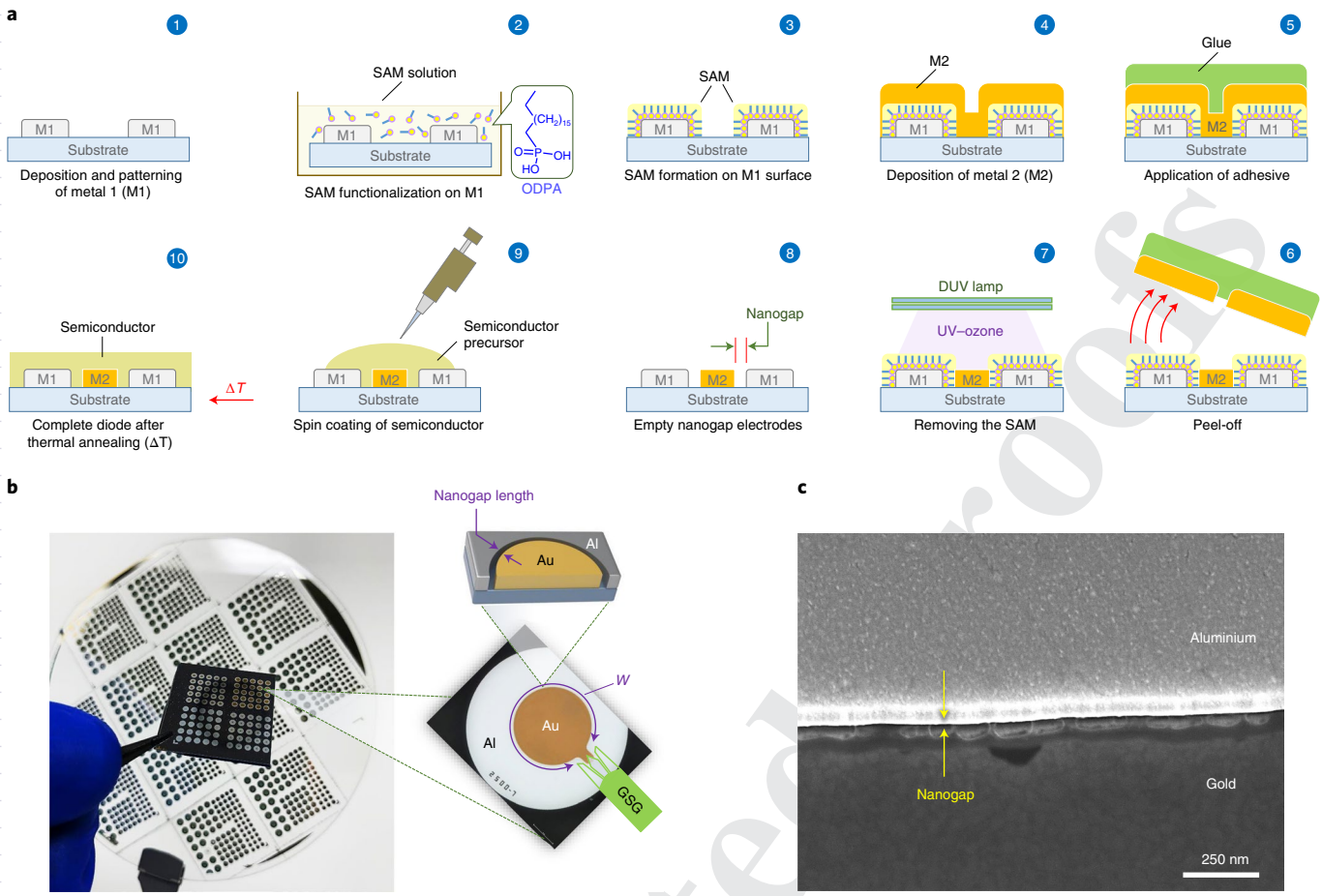

Fig. 1 | Fabrication of nanogap electrodes and radiofrequency Schottky diode structure. a, Generic diagram of adhesion lithography process steps for the fabrication of coplanar asymmetric Al/Au nanogap electrodes: (1) thermal evaporation of Al electrode and patterning to the desired geometry with photolithography, (2) immersion of the patterned substrate in the octadecylphosphonic acid (ODPA) self-assembled monolayer (SAM) solution, (3) ODPA attachment to the native AlO_x of the Al electrode, (4) thermal evaporation of the Au electrode, (5) application of the adhesive glue, (6) removal of the adhesive layer with the excess part of the Au electrode, (7) cleaning the SAM from the Al electrode with ultraviolet (UV)–ozone (DUV, deep ultraviolet), (8) empty coplanar nanogap electrodes, (9) spin coating of the semiconductor precursor and (10) thermal annealing to yield a complete diode device. **b**, Photograph of adhesion-lithography-patterned Al/Au nanogap devices fabricated on a 4-inch wafer and small-scale substrate comprising different electrode widths for scaling studies. Optical micrograph of a 2,500-μm width electrode; the shape was designed to fit the pitch of the microwave probes (G, ground; S, signal) used in the measurement set-up. Schematic of the nanogap device cross-section depicting the nanogap area. **c**, SEM image showing the uniformity of the nanogap separating the two Al and Au electrodes.

A key challenge in developing ultrahigh-frequency Schottky diodes is the ability to simultaneously reduce the junction resistance and capacitance, while retaining the substrate temperature during processing at low levels (<200 °C). In this Article, we report ZnO Schottky diodes that are based on coplanar nanogap (≈15-nm) electrodes—a geometry that allows for significant capacitance reduction by shrinking the active layer thickness to the nanogap channel length, while maintaining the device width on the macroscale. The nanogap electrodes are fabricated using a scalable, high-throughput manufacturing technique called adhesion lithography[11]. We combine our coplanar electrodes with low-cost ZnO and Al-doped ZnO[12] thin films, processed from solution at low temperatures, to boost the radiofrequency response of the diodes to hundreds of gigahertz, while retaining the output voltage at levels close to their peak low-frequency values.

Our nanogap channel geometry reduces the device resistance and capacitance when compared with conventional approaches, thus extending operation to ultrahigh frequencies. The flexibility offered by doping the semiconductor material in its solution phase increases the operating frequency and the output voltage of the rectifier circuits. Furthermore, our fabrication method can be used on different types of substrate and allows for electrode design optimization and monolithic integration of passive components (such as capacitors and resistors, as well as more complicated, multistage rectifier circuits). For example, metal electrodes can be selected on the basis of their work function to match the respective semiconductor energy bands, while the size and geometric pattern of the electrodes can be tailored to the required application (short to operate at mmWave frequencies or longer to deliver higher output voltage, for instance).

Fabrication of planar Schottky diodes

Arrays of asymmetric Al/Au nanogap electrodes were fabricated via adhesion lithography. The process steps are depicted in Fig. 1a and described in detail in Methods. Single devices were fabricated across 4- and 6-inch glass wafers bearing circular structures designed to fit the radiofrequency probes of the measurement set-up (Fig. 1b). Exactly the same process has been transferred to plastic (polyimide)-coated 6-inch glass wafers. In all cases of Au–Al metal combination, the interelectrode distance, that is nanogap

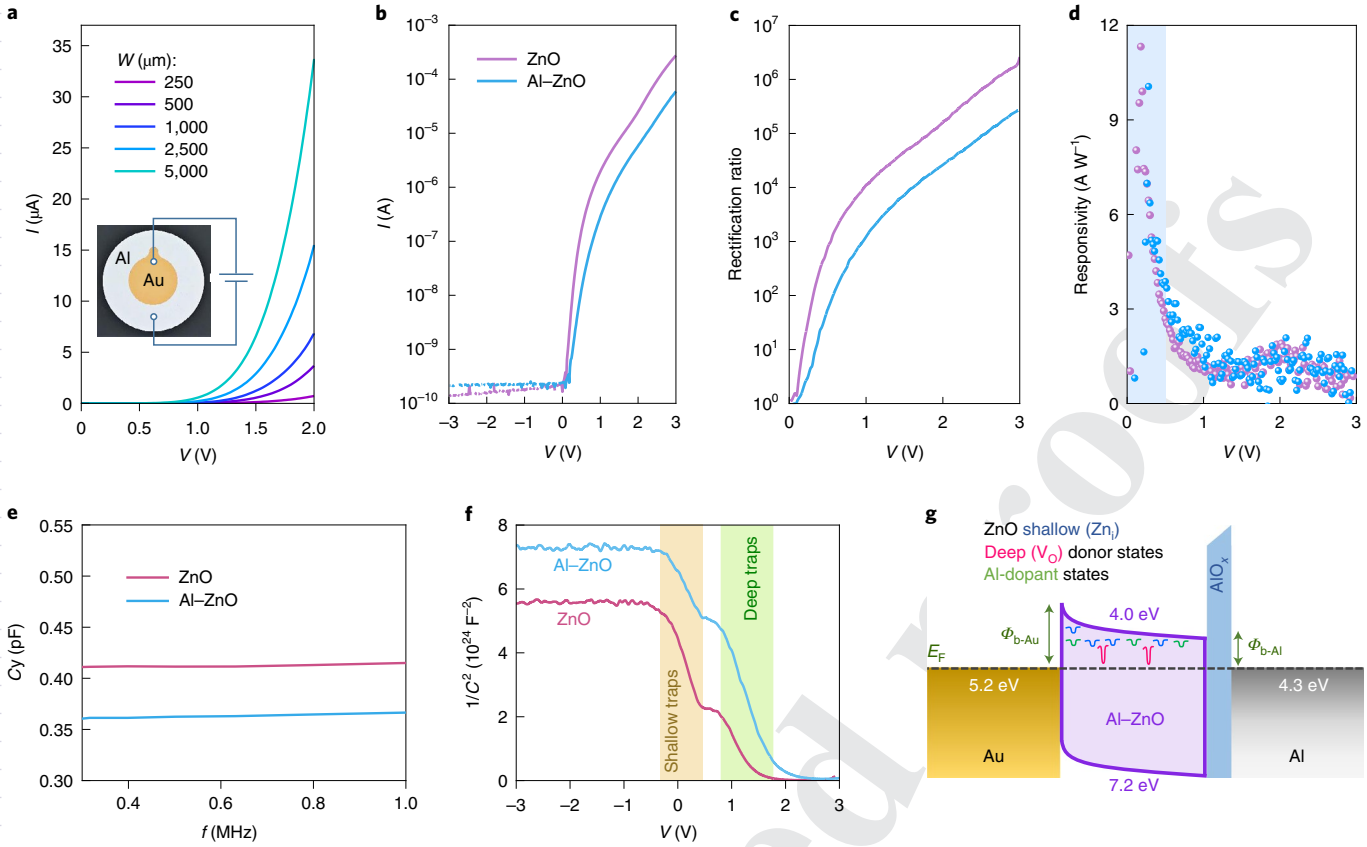

Fig. 2 | D.c. characteristics and operational principle of ZnO and Al–ZnO nanogap Schottky diodes. a, *I*–*V* characteristics of scaled ZnO diodes. Inset: a photograph of a nanogap Al/Au electrode diode. **b**, Semilog *I*–*V* plots of pristine and Al–ZnO Schottky diodes with 1-mm electrode width. **c**,**d**, Rectification ratio (**c**) and quasi-d.c. responsivity (**d**) versus voltage for the same diodes. **e**, *C*–*f* characteristics of the 1-mm ZnO and Al–ZnO diodes. **f**, Mott–Schottky plot derived from *C*–*V* measurements of the same devices at 100 kHz. **g**, Energy band diagram of Au/Al–ZnO/Al diodes depicting defect states in ZnO and the effect of Al.

channel length, *L*, is on average 12.7 ± 3.7 nm (see Supplementary Fig. 1a,d and Supplementary Note 1 for details of the mean nanogap size extraction method). Different metal combinations, such as Ti–Au[11], Al–Al[13], indium tin oxide–Al[14] or Pt–Al (Supplementary Fig. 1b,c,e,f), have also been demonstrated, with nanogap sizes being slightly larger (≈20 nm) than for Au–Al due to the limited process optimization we have performed so far with these metal combinations. The diode width, *W*, is defined by the perimeter of the inner electrode (Fig. 1b and Supplementary Note 2), and is quite homogeneous, showing no significant protrusions or pointed edges along the electrode walls (Fig. 1c and Supplementary Fig. 2), and scales from 250 to 5,000 μm. The semiconductor, pristine ZnO or Al-doped ZnO, was spin coated from an ammonium hydroxide solution on top of the coplanar electrodes and filled the nanogap channel, as also evidenced in the high-resolution transmission electron microscopy (TEM) micrograph and energy-dispersive X-ray spectroscopy elemental mapping (Supplementary Fig. 3).

The low-temperature synthetic route adopted for the growth of ZnO layers from an aqueous precursor solution[15] results in semiconducting layers that contain various electronic defects. These may include oxygen vacancies (V_O) acting as deep donors, Zn interstitials (Zn_i) acting as shallow donors, or Zn vacancies (V_{Zn}), known to exhibit acceptor-like behaviour[16]. To control these defects, we introduce Al into the ZnO lattice following a previously published procedure[12] involving immersion of solid Al pellets in a highly basic ammonium hydroxide ZnO solution to form hydroxoaluminate ($Al(OH)_4^-$) anions. The filtered solution is then spin coated and thermally annealed at 180 °C to result in the Al–ZnO layers (Methods). During annealing, the small Al^{3+} ions, supplied by $Al(OH)_4^-$, are introduced into the ZnO lattice, and can either substitute Zn^{2+} or occupy interstitial sites. This may lead to a concomitant increase in the number of charge carriers but also increase the concentration of lattice defects[17]. Therefore, careful control over the level of doping is of paramount importance to allow the interplay between these two phenomena to be optimized.

D.c. characterization

The current–voltage (*I*–*V*) characteristics of the ZnO Schottky diodes show n-type behaviour, with high nonlinearity and asymmetry and ultralow current in reverse biasing (10^{-10} A), while the current scales linearly with diode width (Fig. 2a and Supplementary Fig. 4)[18]. We performed *I*–*V* measurements on 380 randomly chosen ZnO devices along several areas of a 4-inch substrate (Supplementary Fig. 5a), and the yield of devices showing characteristics similar to those in Fig. 2a,b was 97%, with only 3% being electrically shorted (Supplementary Fig. 5b). The (soft) breakdown of the diodes during d.c. characterization starts around −4 V (Supplementary Fig. 6). However, the diode still shows rectifying behaviour up to >7 V, albeit with reduced rectification ratio (Supplementary Fig. 6a). It should be noted that the breakdown voltage of injected pulses is expected to be up to five times higher than that of injected d.c.[19], which renders these nanogap electrodes functional for high-frequency rectification in low-power electronics applications (see also Supplementary Fig. 6b).

The thickness of both electrodes is 40 nm; therefore, the nominal active area of the coplanar diodes is defined by the electrode width

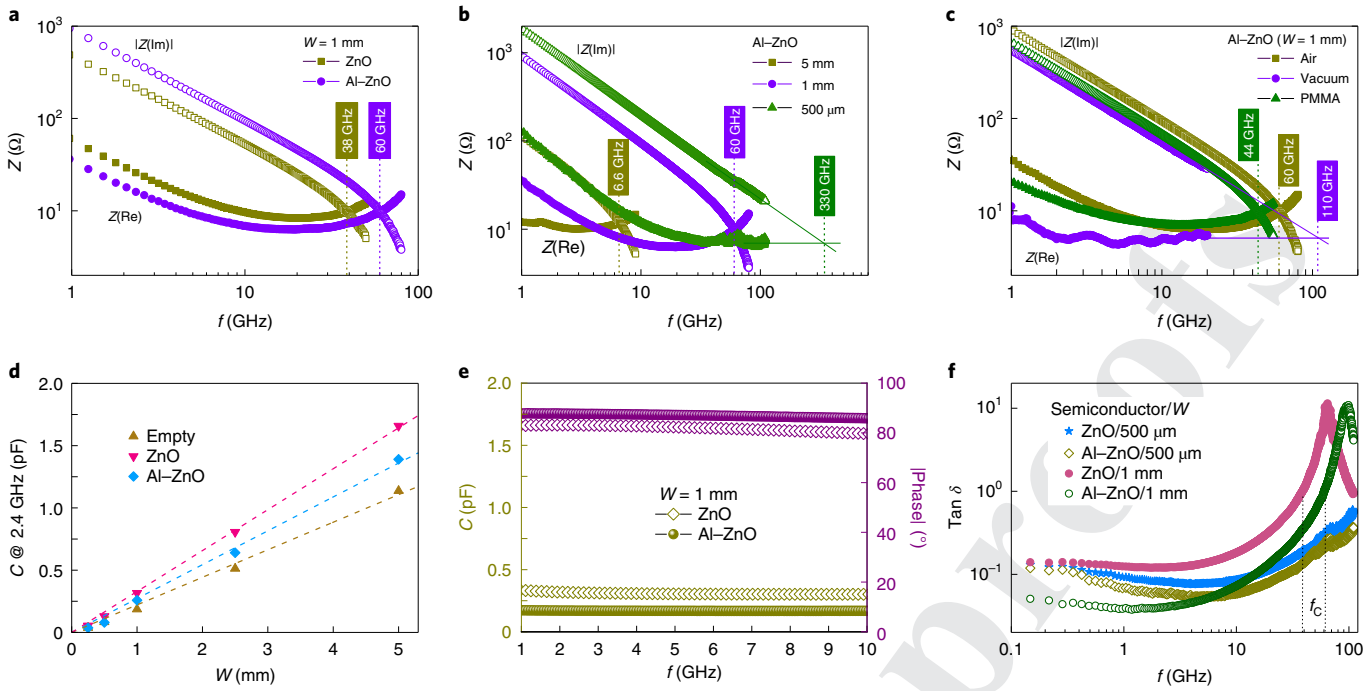

Fig. 3 | High-frequency operation of ZnO-based nanogap Schottky diodes. a–c, Impedance (Z) characteristics of the diodes derived from S_{11} single-port measurements for pristine and Al–ZnO diodes with electrode width of 1 mm (**a**), Al–ZnO diodes with varying electrode widths (500 μm and 1 and 5 mm) (**b**), and environmental stability of non-encapsulated Al–ZnO diodes measured in air and in vacuum and PMMA-encapsulated devices measured in air (**c**). The cutoff frequency is defined at the intersection of the real and imaginary parts of the impedance. **d–f**, High-frequency capacitance studies of the pristine and Al–ZnO diodes: **d**, capacitance versus electrode-width scaling study of the empty nanogaps and pristine and Al–ZnO diodes at 2.4-GHz frequency; **e**, capacitance and phase response of the 1-mm-width pristine and Al–ZnO diodes in the 1–10-GHz range; **f**, tan δ for the same 1-mm- and for 500-μm-width pristine and Al–ZnO diodes (arrows indicate the f_C of the 1-mm devices).

(250–5,000 μm) multiplied by its thickness, resulting in device areas ranging from 10 to 200 μm^2. The Al electrode serves as the Ohmic contact because of the small work-function difference between the Fermi level of Al (4.3 eV) and the conduction-band edge of ZnO (4.0 eV). The Au electrode forms a Schottky contact due to its high work function of 5.2 eV, establishing a 1.2-eV Schottky barrier with the conduction band of ZnO[9].

The I–V characteristics of pristine and Al–ZnO diodes are highly asymmetric (Fig. 2b), showing large rectification ratios of $>10^5$ (Fig. 2c) and high nonlinearities in the measured voltage range (Supplementary Fig. 7), both of which are critical for high-frequency rectification. This electrical behaviour is quite repeatable and shows very small device-to-device variability in ZnO and Al–ZnO diodes (Supplementary Fig. 8). These exceptional electrical characteristics attest that the electrical field is homogeneously distributed along the nanogap walls, indicating a small wall roughness, as also evidenced by the scanning electron microscopy (SEM) images. Also of particular relevance, especially for radiofrequency energy-harvesting applications, is the current responsivity of the diode. This is proportional to the ratio of the second derivative of the I–V curve (d^2I/dV^2) to the differential conductance (dI/dV) and provides a measure of the rectified output d.c. for a given input radiofrequency power (Supplementary Note 3)[20]. For efficient energy harvesting, it is important to have high current responsivity at very low (close to zero) applied bias. Here, we calculate the low-level quasistatic d.c. responsivities of 11 A W^{-1} at 0.18 V and 10 A W^{-1} at 0.28 V, very close to the diodes' turn-on voltage, for the pristine and Al–ZnO diodes, respectively (Fig. 2d). These values are much higher than the ones reported recently for MoS_2 flexible rectifiers (4.7 A W^{-1}; ref. [21]) and similar to those of SiC–graphene Schottky diodes[7].

The ideality factor derived from the I–V curves for both pristine and Al–ZnO diodes (Fig. 2b and Supplementary Table 1) deviates from 1, strongly suggesting the presence of interfacial states in the bandgap and/or mechanisms other than thermionic emission. The small decrease in conductivity and the slightly increased reverse current imply the incorporation of Al atoms also at interstitial sites, providing holes and adding extra acceptor levels in the bandgap, close to the valence band. Indeed, the series resistance, R_S, as estimated from the Cheung plots (Supplementary Fig. 9 and Supplementary Note 4), increases from 140 to 220 kΩ. This is further corroborated from impedance measurements. The capacitance measured as a function of frequency (C–f) shows a plateau at low frequencies, with the Al–ZnO ($W \approx 1{,}000$ μm) diode exhibiting a capacitance value of 0.36 pF, as compared with the pristine ZnO one, which is ≈0.41 pF (Fig. 2e). These values are corrected by subtracting the capacitance of the empty electrode (0.2 pF; ref. [9]) from the initially measured values. The low capacitance values indicate that charges are able to respond promptly to the change of the alternating field applied during the measurement (that is, less charge is stored), rendering them particularly attractive for high-frequency applications.

Taking into account the extrinsic capacitance contribution due to 3D coupling of the coplanar electrodes and applying the conformal mapping technique (Supplementary Note 5), we calculate relative dielectric constants in the range of $\varepsilon \approx 10$–12, in accordance with previous reports on crystalline ZnO films[22,23]. The Mott–Schottky plots (Fig. 2f) derived from C–V measurements (see also Supplementary Fig. 10 for C–V at different frequencies), corrected for the empty electrode contribution, comprise two distinct linear voltage ranges with negative slopes, separated by a plateau at $V_p \approx 0.6$ V, where $V < V_p$ indicates shallow levels (that is, closer to the

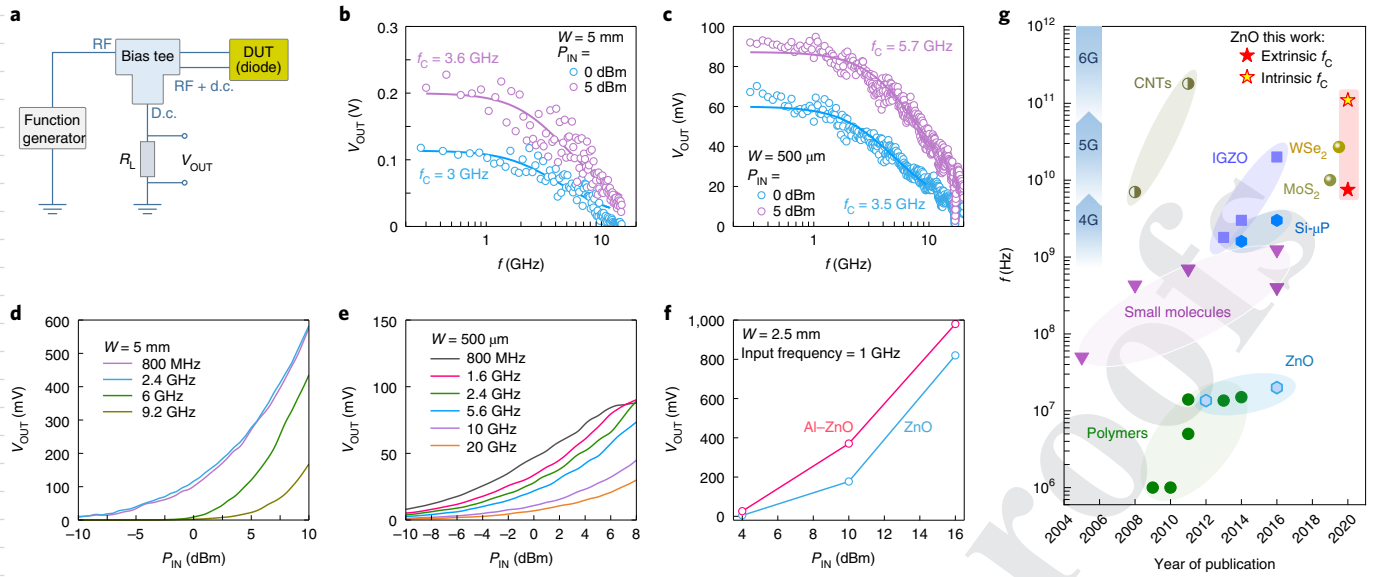

Fig. 4 | Output-voltage capabilities of the ZnO-based rectifier. a, Circuit diagram of the measurement set-up of the single-stage rectifier, comprising a bias tee and a load resistor. RF, radiofrequency. **b**–**e**, Output voltage as a function of frequency for input radiofrequency power of 0 and 5 dBm (**b**,**c**) and of input radiofrequency power at certain frequencies of interest (**d**,**e**), for the ZnO diodes with electrode width of 5 mm (**b**,**d**) and 500 μm (**c**,**e**). Cutoff frequencies in **b**,**c** are calculated upon fitting the transfer function for the RC low-pass filter to the experimental data. **f**, Comparison of output voltage versus input radiofrequency power for the pristine and Al–ZnO diodes with 2.5-mm electrode width at 1 GHz. The lines are guides to the eye. **g**, Frequency performance comparison of state-of-the-art Schottky diodes comprising different materials with the best ZnO-based diodes shown here (see Supplementary Table 3 for full details of device structure, fabrication method and extrinsic/intrinsic cutoff frequency performance). CNTs, carbon nanotubes; IGZO, indium gallium zinc oxide; Si-μP, silicon microparticles.

conduction band) and $V > V_p$ deep donor levels (closer to the Fermi level)[24]. From the Mott–Schottky analysis, we find that the concentration of shallow traps increases (from 2.2 to 3.5×10^{19} cm^{-3}), while that of deep traps decreases (from 3.6 to 2.3×10^{19} cm^{-3}) in the Al–ZnO film as compared with ZnO (Supplementary Note 6 and Supplementary Table 1). A plausible explanation is that AlO_2^- fills some of the deep traps, while Al^{3+} ions substituting Zn^{2+} provide extra electrons at shallow donor levels (Fig. 2g). Deep traps generally result in lower conductivity as they are states heavily occupied by charges. Shallow traps show strong kinetic dependence and may be classified as slow or fast on the basis of their trap capture and release time being shorter or longer than the transit time, respectively[25]. In the presence of fast traps, all charge carriers are being repeatedly trapped and released when travelling through the device, effectively increasing the transit time and lowering the mobility. This poses a limit in the cutoff frequency of the diodes as the resistance value is increased (as compared with a trap-free diode). In the case of slow traps, on the other hand, charge carriers are able to cross the semiconductor layer and reach the collecting contact before being trapped[26]. The effect of slow shallow traps is particularly beneficial at high frequencies (that is, when the signal period is much shorter than the electron transit time), as they resemble the ideal trap-free diode characteristics and lead to increased cutoff frequencies[27].

Scattering-parameter analysis

The microwave and mmWave frequency response of the ZnO diodes was investigated by measuring the one-port scattering (S) parameters. The input reflection coefficients (S_{11}) (ratio of reflected to incident waves) were measured and the capacitive and resistive components of the complex impedance were extracted. The intrinsic cutoff frequency, f_C, is determined at the intersection of the real (resistance) and imaginary (reactance) parts of the impedance, and signifies the highest frequency at which signals are propagated. It refers to the intrinsic speed of the diode, as defined by the junction resistance, junction capacitance and series resistance values, while it neglects any transmission losses, load resistance and impedance-matching losses, usually present in actual rectifier circuits. Note that the resistances (real part of impedance) shown here are orders of magnitude different from the ones calculated from d.c. (Cheung) plots, as the former actually represent the effective resistance, R_{ES} (ref. [28]). This is the total series resistance R minus the resistance of the depletion region. Since at ultrahigh frequencies (>1 GHz), and for close to zero biasing, the semiconductor layer is expected to be fully depleted, R_{ES} is effectively reflecting the contribution of the Ohmic contact resistance of the metal/semiconductor interface (see Supplementary Table 2 for the radiofrequency parameter values extracted from Fig. 3a,b).

For a diode width of 1 mm, f_C values as high as 38 and 60 GHz were measured at an input power of −8 dBm for the ZnO and Al–ZnO diodes, respectively (Fig. 3a). This finding is in line with the capacitance study above, indicating that Al doping decreases the concentration of deep traps, while simultaneously increasing the density of slow shallow trap states, which is expected to favour ultrahigh-frequency operation[27].

Next, we focus on the best-performing Al–ZnO diodes and investigate the role of the geometrical parameters by scaling the electrodes' width to 500 μm and 1 and 5 mm. As expected, the high-frequency response of the smallest (500-μm)-width electrodes outperforms that of the larger ones, reaching a cutoff frequency in the hundreds of gigahertz (note that the limit of our vector network analyser (VNA) characterization set-up was 110 GHz) (Fig. 3b). We investigated the environmental stability of the nanogap devices by measuring in air and in vacuum. Notwithstanding the fact that the VNA instrument operating in the vacuum chamber had a maximum applied frequency of 20 GHz, it is evident that an oxygen-deficient environment is beneficial to device performance (Supplementary Fig. 11). Adding a capping (poly(methyl methacrylate), PMMA)

layer on top of the semiconductor improves device d.c. temporal stability (Supplementary Fig. 12) with the trade-off of reduced cut-off frequency due to the excess capacitance induced by the top layer (Fig. 3c and Supplementary Fig. 13).

The junction capacitance is instrumental in maximizing the cutoff frequency and the high-frequency response in general. We address this from the material and electrode geometry viewpoint. The capacitance at the Bluetooth- and Wi-Fi-relevant frequency of 2.45 GHz scales linearly for both pristine and Al–ZnO diodes (Fig. 3d). By scaling the electrode width at will, we can match the diode capacitance to that of the antenna in a rectenna circuit. The same trend holds for the empty-nanogap electrodes, emphasizing the effect of geometrical area on performance optimization; however, the capacitance values are slightly lower in empty electrodes, most likely due to the lower dielectric constant of air filling the space in the nanogap. The capacitance of the 1-mm ZnO and Al–ZnO diodes exhibits remarkable stability over the 1–10-GHz frequency range and retains its phase close to 90°, indicative of a high-quality low-k material, where the major contribution to the dielectric constant originates from electronic polarization (Fig. 3e)[29]. Upon analysing further the dielectric properties of the ZnO (filled symbols in Fig. 3f) and Al–ZnO (open symbols), over the entire frequency range of 0.1 to 110 GHz, we observe that the dissipation factor, expressed as the loss tangent, $\tan\delta$, is higher for the ZnO as compared with Al–ZnO, reinforcing its suitability for ultrahigh-frequency applications. The absence of peaks in the higher-frequency regime for the smaller-diode-width devices (500 µm versus 1 mm) indicates that the hopping frequency of the localized electric charge carriers is higher than 110 GHz.

Rectifier circuit

The extrinsic f_C of a Schottky diode is a more direct way of evaluating the rectifier performance at the system level, as it is measured directly through the rectifier circuit, which is closer to practical applications. It is conventionally defined at the '−3 dB point', which refers to the frequency at which the power absorbed by the diode drops by half (or the output voltage, V_{OUT}, drops to $1/\sqrt{2}$) of its peak output power (or V_{OUT}) at low frequency[30]. A simple analysis derived from the transfer function for an RC low-pass filter leads to the following expression for V_{OUT} versus frequency from which the cutoff frequency may be determined (Supplementary Note 7):

$$V_{OUT} = \frac{V_0}{\sqrt{1 + \left(\frac{f}{f_C}\right)^2}}$$

The output voltage as a function of frequency was measured using a half-wave rectifier set-up, comprising a bias tee and a 15-MΩ load resistor, R_L (Fig. 4a). The ZnO diodes with 5,000-µm electrode width show a maximum cutoff frequency of 3.6 GHz at 5 dBm input power (Fig. 4b). Reducing the diode size to 500-µm electrode width (Fig. 4c), the cutoff frequency increases to 5.7 GHz at 5 dBm. More interestingly, both larger and smaller diodes have a cutoff frequency well above the Wi-Fi and Bluetooth benchmark frequency of 2.45 GHz at 0 dBm (3 and 3.5 GHz, respectively), which opens up the application landscape of these devices to wireless energy-harvesting systems.

The output voltage as a function of input radiofrequency power follows a square law with two linear regions discernible for all frequencies (Fig. 4d,e). From these graphs, we can also estimate cutoff frequencies of 6 GHz for 5 mm at 10 dBm and around 7.5 GHz for 500 µm at 8 dBm. V_{OUT} scales with size, as expected, and is around 600 mV for the larger diode at 10 dBm and 90 mV for the smaller diode at 5 dBm of input radiofrequency power (Fig. 4e) at frequencies up to 2.4 GHz. However, even at much higher frequencies of 10 GHz, the 5 mm and 500 µm devices still output voltages of around 250 mV and 45 mV, respectively (at 8–10 dBm input). Substituting the ZnO with Al–ZnO diodes further increases the output voltage, as evidenced from measurements at high frequencies of 13.56 MHz (Supplementary Fig. 14). More interestingly, at 1 GHz the 2.5-mm-width Al-doped ZnO devices show a more than twofold increase in their V_{OUT}, namely 370 mV at 10 dBm input radiofrequency power (P_{IN}), as compared with the ZnO diodes of the same size, which output a voltage of 180 mV (Fig. 4f).

Conclusions

The high intrinsic and extrinsic cutoff frequencies (>100 GHz and >7 GHz, respectively) of our diodes improve on those based on vacuum-processed[28,31] and solution-processed metal oxides[10,32–34] as well as on devices based on silicon microparticles[35,36] (Fig. 4g and Supplementary Table 3). Using simple and scalable manufacturing processes, our diodes are able to compete directly with state-of-the-art radiofrequency Schottky devices based on a variety of nanomaterials, including carbon nanotubes[37–39], graphene oxide[40], MoS_2[21] and WSe_2[41], while approaching the performance of complementary metal–oxide–semiconductor (CMOS)-integrated Schottky diodes on silicon[42,43]. Our approach also offers the advantage of not compromising performance for reliable manufacturing and cost constraints. Furthermore, adhesion lithography offers the possibility of monolithic integration of active components (diodes) with a variety of passive components, such as antennas, capacitors and resistors, or the design of charge-pumping circuits, such as voltage multipliers and Delon circuits to increase the output voltage of an individual rectifier. This technology could address the need for device-level scalability in a 'more than Moore' strategy[44], and can be considered a new circuit-design approach for emerging device ecosystems, such as Internet of Things systems based on future wireless standards (5G and 6G).

Methods

Fabrication of nanogap electrodes. Coplanar nanogap separated electrodes were patterned with adhesion lithography. An Al electrode with a thickness of 40 nm was thermally evaporated in high vacuum (10^{-6} mbar) on 4- or 6-inch glass or polyimide-coated glass wafer and patterned to the desired design with photolithography, followed by wet etching. The patterned substrates were soaked in a 1-mM solution of octadecylphosphonic acid (Sigma Aldrich) in isopropanol to form a SAM on the Al surface, rendering it hydrophobic. Next, a global Au electrode (35 nm), with a 5-nm Al underlayer to promote adhesion to the glass substrate, was deposited via thermal evaporation. An adhesive film (First Contact, Photonic Cleaning Technologies) was applied with a brush on the small substrates or spray coated on the wafer and left to dry in air for about 20 min. Then, the adhesive glue was peeled off using a tape, removing the Au metal from the top of the SAM-functionalized Al. A second photolithography and wet etching step was then performed to isolate each diode from the global Al electrode on the substrate. The SAM and any remaining photoresist were cleaned via a 15-min ultraviolet–ozone treatment to reveal an empty nanogap, typically of the order of 15 nm.

ZnO and Al-doped ZnO formulations and film deposition. Precursor solution of undoped ZnO was prepared by dissolving zinc oxide powder (99.99% trace-metal basis, Sigma Aldrich) in ammonium hydroxide (50% v/v aqueous, Alfa Aesar) at a concentration of 10 mg ml^{-1}. For the Al-doped ZnO, a 3-mm-diameter Al pellet (99.999% purity, Lesker) was immersed in 8 ml of the above ZnO solution and left for 7 min. The pellet was then removed, and the solution was filtered with a 0.45-µm polytetrafluoroethylene filter. The respective solution (undoped or doped) was spin coated directly onto the substrates prepatterned with the nanogap electrodes at 4,000 r.p.m. for 40 s followed by 35 min thermal annealing at 180 °C in air. A second layer of the same solution was spin coated following exactly the same procedure. The PMMA (relative molecular mass 120,000, Sigma Aldrich) film that was used as encapsulant was spin coated from its 40-mg-ml^{-1} solution in butyl acetate at 2,000 r.p.m. for 40 s and annealed at 125 °C for 30 min inside a N_2-filled glovebox.

Scanning and transmission electron microscopy. Top-view SEM images of the Al/Au nanogap were acquired with the help of a Helios G4 UX microscope equipped with a field emission electron source at the operating voltage of 5 kV. To acquire the cross-sectional images first a thin lamella was prepared with the focused ion beam (FIB) in a scanning electron microscope (Helios 400 s, FEI) equipped with a nanomanipulator (Omniprobe AutoProbe300). The sample's surface was protected by sequential layers of carbon and platinum deposited under the electron and ion beams. The bulk of the sample was milled with the Ga ion beam to reach a depth

of about 8–10 µm. The U-cut was made with the FIB and then the lamella was extracted from the bulk according to the lift-out method. The lamella attached to a copper TEM grid was then thinned down with the FIB at 30 kV and sequentially reducing current in the range of 2.8 nA–93 pA. Finally the lamella was polished with the FIB at low voltages (5 and 2 kV) to remove any possible contamination. Then the cross-sectional images were acquired with the TEM (Titan 80–300, FEI) at 300 kV operating voltage. The energy-dispersive X-ray spectra were acquired in the scanning TEM mode with a Quantum 966 Gatan imaging filter.

Electrical characterization. *I–V* characterization of the diodes was carried out on an Agilent B2902A parameter analyser and capacitance measurements were recorded with a Solartron 1260 impedance analyser at room temperature inside a N_2-filled glovebox. *I–V* scans (−2 to 2 V) were performed on 380 randomly chosen devices from the 4-inch substrate coated with ZnO using the Automated Characterization Suite (V4.4) of a Keithley 4200A-SCS parameter analyser connected to a Wentworth Laboratories probe station. Statistical analysis was carried out on the *I–V* measurements: devices showing currents $>10^{-4}$ A were considered shorted (FAIL) and those in the current range 10^{-9}–10^{-6} A were considered functional diodes (PASS). High-frequency measurements were obtained either through an Agilent PNA-L N5230A (300-kHz–20-GHz) VNA with samples placed inside a vacuum-sealed chamber (4×10^{-3} mbar) or in ambient through an Agilent PNA E8361C VNA with Agilent N5260-60003 extender modules operating at 10 MHz–110 GHz. The power detector circuit was designed by performing LT SPICE simulations to measure the output voltage of the rectifier (Fig. 4a). A signal generator (Agilent E8257D, 250 MHz to 50 GHz) was connected to the bias tee and the output voltage was measured across a load resistor $R_L = 15$ MΩ, whose value is chosen to obtain maximum V_{OUT}. Cascade Infinity GSG probes were used in all frequency measurements.

Data availability

The data that support the plots within this paper and other findings of this study are available from the corresponding authors upon reasonable request.

Received: 17 March 2020; Accepted: 9 September 2020;

References

1. Kim, D. & Zarri, M. (eds) *Road to 5G: Introduction and Migration* (GSMA, 2018).
2. Ilderem, V. The technology underpinning 5G. *Nat. Electron.* **3**, 5–6 (2020).
3. Dang, S., Amin, O., Shihada, B. & Alouini, M.-S. What should 6G be? *Nat. Electron.* **3**, 20–29 (2020).
4. Yang, P., Xiao, Y., Xiao, M. & Li, S. 6G wireless communications: vision and potential techniques. *IEEE Netw.* **33**, 70–75 (2019).
5. Ni, Y., Liang, J., Shi, X. & Ban, D. Research on key technology in 5G mobile communication network. In *2019 International Conference on Intelligent Transportation, Big Data & Smart City (ICITBS)* 199–201 (IEEE, 2019).
6. Nagatsuma, T., Ducournau, G. & Renaud, C. C. Advances in terahertz communications accelerated by photonics. *Nat. Photonics* **10**, 371–379 (2016).
7. Schlecht, M. T., Preu, S., Malzer, S. & Weber, H. B. An efficient terahertz rectifier on the graphene/SiC materials platform. *Sci. Rep.* **9**, 11205 (2019).
8. Zhang, J. et al. Room temperature processed ultrahigh-frequency indium–gallium–zinc–oxide Schottky diode. *IEEE Electron Device Lett.* **37**, 389–392 (2016).
9. Semple, J. et al. Radio frequency coplanar ZnO Schottky nanodiodes processed from solution on plastic substrates. *Small* **12**, 1993–2000 (2016).
10. Park, H. et al. Fully roll-to-roll gravure printed rectenna on plastic foils for wireless power transmission at 13.56 MHz. *Nanotechnology* **23**, 344006 (2012).
11. Beesley, D. J. et al. Sub-15-nm patterning of asymmetric metal electrodes and devices by adhesion lithography. *Nat. Commun.* **5**, 3933 (2014).
12. Lin, Y.-H. et al. Al-doped ZnO transistors processed from solution at 120 °C. *Adv. Electron. Mater.* **2**, 1600070 (2016).
13. Semple, J., Wyatt-Moon, G., Georgiadou, D. G., McLachlan, M. A. & Anthopoulos, T. D. Semiconductor-free nonvolatile resistive switching memory devices based on metal nanogaps fabricated on flexible substrates via adhesion lithography. *IEEE Trans. Electron Devices* **64**, 1973–1980 (2017).
14. Georgiadou, D. G. et al. High responsivity and response speed single-layer mixed-cation lead mixed-halide perovskite photodetectors based on nanogap electrodes manufactured on large-area rigid and flexible substrates. *Adv. Funct. Mater.* **29**, 1901371 (2019).
15. Lin, Y.-H. et al. High-performance ZnO transistors processed via an aqueous carbon-free metal oxide precursor route at temperatures between 80–180 °C. *Adv. Mater.* **25**, 4340–4346 (2013).
16. Janotti, A. & Van de Walle, C. G. Fundamentals of zinc oxide as a semiconductor. *Rep. Prog. Phys.* **72**, 126501 (2009).
17. Zamiri, R., Singh, B., Scott Belsley, M. & Ferreira, J. M. F. Structural and dielectric properties of Al-doped ZnO nanostructures. *Ceram. Int.* **40**, 6031–6036 (2014).
18. Georgiadou, D. G., Semple, J. & Anthopoulos, T. D. Adhesion lithography for fabrication of printed radio-frequency diodes. *SPIE Newsroom* https://www.spie.org/news/6783-adhesion-lithography-for-fabrication-of-printed-radio-frequency-diodes?SSO=1 (2017).
19. Meng, G., Cheng, Y., Wu, K. & Chen, L. Electrical characteristics of nanometer gaps in vacuum under direct voltage. *IEEE Trans. Dielectr. Electr. Insul.* **21**, 1950–1956 (2014).
20. Hemour, S. & Wu, K. Radio-frequency rectifier for electromagnetic energy harvesting: development path and future outlook. *Proc. IEEE* **102**, 1667–1691 (2014).
21. Zhang, X. et al. Two-dimensional MoS_2-enabled flexible rectenna for Wi-Fi-band wireless energy harvesting. *Nature* **566**, 368–372 (2019).
22. Kim, H. K. & Mathur, M. Structural and electrical properties of ZnO films deposited on GaAs substrates by RF magnetron sputtering. *MRS Proc.* **238**, 317 (1991).
23. Alexander, T. P. et al. Dielectric properties of sol–gel derived ZnO thin films. in *ISAF '96. Proc. 10th IEEE International Symposium on Applications of Ferroelectrics* Vol. 2, 585–588 (IEEE, 1996).
24. Almora, O., Aranda, C., Mas-Marzá, E. & Garcia-Belmonte, G. On Mott–Schottky analysis interpretation of capacitance measurements in organometal perovskite solar cells. *Appl. Phys. Lett.* **109**, 173903 (2016).
25. Knapp, E. & Ruhstaller, B. The role of shallow traps in dynamic characterization of organic semiconductor devices. *J. Appl. Phys.* **112**, 024519 (2012).
26. Montero, J. M., Bisquert, J., Garcia-Belmonte, G., Barea, E. M. & Bolink, H. J. Trap-limited mobility in space-charge limited current in organic layers. *Org. Electron.* **10**, 305–312 (2009).
27. Dascălu, D. Trapping and transit-time effects in high-frequency operation of space-charge-limited dielectric diodes: frequency characteristics. *Solid-State Electron.* **11**, 491–499 (1968).
28. Zhang, J. et al. Flexible indium–gallium–zinc–oxide Schottky diode operating beyond 2.45 GHz. *Nat. Commun.* **6**, 7561–7561 (2015).
29. Wang, B. et al. High-*k* gate dielectrics for emerging flexible and stretchable electronics. *Chem. Rev.* **118**, 5690–5754 (2018).
30. Semple, J., Georgiadou, D. G., Wyatt-Moon, G., Gelinck, G. & Anthopoulos, T. D. Flexible diodes for radio frequency (RF) electronics: a materials perspective. *Semicond. Sci. Technol.* **32**, 123002 (2017).
31. Chasin, A. et al. An integrated a-IGZO UHF energy harvester for passive RFID tags. *IEEE Trans. Electron Devices* **61**, 3289–3295 (2014).
32. Lin, C.-Y. et al. High-frequency polymer diode rectifiers for flexible wireless power-transmission sheets. *Org. Electron.* **12**, 1777–1782 (2011).
33. Heljo, P., Lilja, K. E., Majumdar, H. S. & Lupo, D. High rectifier output voltages with printed organic charge pump circuit. *Org. Electron.* **15**, 306–310 (2014).
34. Li, M. et al. 0.7-GHz solution-processed indium oxide rectifying diodes. *IEEE Trans. Electron Devices* **67**, 360–364 (2020).
35. Sani, N. et al. All-printed diode operating at 1.6 GHz. *Proc. Natl Acad. Sci. USA* **111**, 11943–11948 (2014).
36. Sani, N. et al. Flexible lamination-fabricated ultrahigh frequency diodes based on self-supporting semiconducting composite film of silicon micro-particles and nano-fibrillated cellulose. *Sci. Rep.* **6**, 28921 (2016).
37. Manohara, H. M., Wong, E. W., Schlecht, E., Hunt, B. D. & Siegel, P. H. Carbon nanotube Schottky diodes using Ti–Schottky and Pt–Ohmic contacts for high frequency applications. *Nano Lett.* **5**, 1469–1474 (2005).
38. Cobas, E. & Fuhrer, M. S. Microwave rectification by a carbon nanotube Schottky diode. *Appl. Phys. Lett.* **93**, 043120 (2008).
39. Yang, X. & Chahal, P. Large-area low-cost substrate compatible CNT Schottky diode for THz detection. In *2011 IEEE 61st Electronic Components and Technology Conference (ECTC)* 2158–2164 (IEEE, 2011).
40. Kaur, A., Yang, X., Park, K. Y. & Chahal, P. Reduced graphene oxide based Schottky diode on flex substrate for microwave circuit applications. In *2013 IEEE 63rd Electronic Components and Technology Conference* 1037–1042 (IEEE, 2013).
41. Yang, S. J. et al. Ultrafast 27 GHz cutoff frequency in vertical WSe_2 Schottky diodes with extremely low contact resistance. *Nat. Commun.* **11**, 1574 (2020).
42. Mishra, C., Pfeiffer, U., Rassel, R. & Reynolds, S. Silicon Schottky diode power converters beyond 100 GHz. In *2007 IEEE Radio Frequency Integrated Circuits (RFIC) Symposium* 547–550 (IEEE, 2007).
43. Sankaran, S. & O, K. K. Schottky diode with cutoff frequency of 400 GHz fabricated in 0.18 µm CMOS. *Electron. Lett.* **41**, 506–508 (2005).
44. Son, Y., Frost, B., Zhao, Y. & Peterson, R. L. Monolithic integration of high-voltage thin-film electronics on low-voltage integrated circuits using a solution process. *Nat. Electron.* **2**, 540–548 (2019).

Acknowledgements

D.G.G., J.S. and T.D.A. acknowledge financial support from the European Union Horizon 2020 research and innovation programme under the Marie Skłodowska-Curie grant agreement 706707, the European Research Council (ERC) project AMPRO under grant number 280221, the Engineering and Physical Sciences Research Council (EPSRC) grant number EP/P505550/1 and the EPSRC Centre for Innovative Manufacturing in

Large Area Electronics (CIM-LAE) grant number EP/K03099X/1. A.S., K.L., H.F. and T.D.A. acknowledge support by the King Abdullah University of Science and Technology (KAUST) Office of Sponsored Research (OSR) under award number OSR-2018-CARF/CCF-3079. A.A.S. thanks SERB for an Early Research Career Award (ECR/2017/1562) and SRM IST for financial support. We also thank S. Kano for helpful discussion on the nanogap size analysis.

Author contributions

T.D.A., D.G.G. and J.S. conceived the project. T.D.A. guided and supervised the project. D.G.G. and J.S. fabricated the small-scale devices and performed electrical measurements. D.G.G. analysed the data. A.A.S. set up the high-frequency rectifier circuit measurements and D.G.G., J.S. and A.A.S. analysed the data. D.G.G., H.F. and P.R. performed the single-port measurements and extracted and analysed the data. Y.-H.L. provided the Al-doped ZnO formulations. A.S., K.L. and H.F. carried out SEM and TEM characterization and performed statistical analysis on data derived from microscopy images. F.A. assisted with fabrication of wafer-scale devices and their electrical characterization. D.G.G. and T.D.A. wrote the first draft of the manuscript. All authors discussed the results and contributed to the final version of the paper.

Competing interests

The authors declare no competing interests.

Additional information

Supplementary information is available for this paper at https://doi.org/10.1038/s41928-020-00484-7.

Correspondence and requests for materials should be addressed to D.G.G. or T.D.A.

Reprints and permissions information is available at www.nature.com/reprints.

Publisher's note Springer Nature remains neutral with regard to jurisdictional claims in published maps and institutional affiliations.

QUERY FORM

Nature Electronics	
Manuscript ID	**[Art. Id: 484]**
Author	**Dimitra G. Georgiadou**

AUTHOR:

The following queries have arisen during the editing of your manuscript. Please answer by making the requisite corrections directly in the e.proofing tool rather than marking them up on the PDF. This will ensure that your corrections are incorporated accurately and that your paper is published as quickly as possible.

Query No.	*Nature of Query*
Q1:	Please check your article carefully, coordinate with any co-authors and enter all final edits clearly in the eproof, remembering to save frequently. Once corrections are submitted, we cannot routinely make further changes to the article.
Q2:	Note that the eproof should be amended in only one browser window at any one time; otherwise changes will be overwritten.
Q3:	Author surnames have been highlighted. Please check these carefully and adjust if the first name or surname is marked up incorrectly. Note that changes here will affect indexing of your article in public repositories such as PubMed. Also, carefully check the spelling and numbering of all author names and affiliations, and the corresponding email address(es).
Q4:	You cannot alter accepted Supplementary Information files except for critical changes to scientific content. If you do resupply any files, please also provide a brief (but complete) list of changes. If these are not considered scientific changes, any altered Supplementary files will not be used, only the originally accepted version will be published.
Q5:	Please note, we reserve 'significant' and its derivatives for statistical significance. Please reword where this is not the intended meaning (for example to important, notable, substantial); there are three instances throughout your text.
Q6:	In the sentence beginning "Different metal combinations...", please confirm that the insertion of "indium tin oxide" as the definition of "ITO" is correct.
Q7:	In Fig. 1a(7) caption, please confirm that the insertion of "deep ultraviolet" as the definition of "DUV" is correct.
Q8:	In Fig. 4g caption, please confirm that the insertion of "silicon microparticles" as the definition of "Si-μP" is correct.
Q9:	In the sentence beginning "Using simple and scalable...", please confirm that the insertion of "complementary metal–oxide–semiconductor" as the definition of "CMOS" is correct.
Q10:	In the sentence beginning "This technology...", please confirm that the insertion of "Internet of things" as the definition of "IoT" is correct.
Q11:	In the sentence beginning "The pellet...", please confirm that the insertion of "polytetrafluoroethylene" as the definition of "PTFE" is correct.

QUERY FORM

Nature Electronics	
Manuscript ID	**[Art. Id: 484]**
Author	**Dimitra G. Georgiadou**

AUTHOR:

The following queries have arisen during the editing of your manuscript. Please answer by making the requisite corrections directly in the e.proofing tool rather than marking them up on the PDF. This will ensure that your corrections are incorporated accurately and that your paper is published as quickly as possible.

Query No.	*Nature of Query*
Q12:	In the sentence beginning "The PMMA...", please confirm that the insertion of "relative molecular mass" to replace "MW" is correct.